



TECHNICAL ARTICLE

# On Development of Alternating Layer Acrylonitrile Butadiene Styrene-Al Composite Structures Using Additive Manufacturing

*Piyush, Raman Kumar, Ranvijay Kumar, Nishant Ranjan, and Jasgurpreet Singh Chohan*

Submitted: 27 October 2021 / Revised: 11 March 2022 / Accepted: 18 March 2022 / Published online: 26 April 2022

Fused filament fabrication (FFF) is one of the low-cost 3D printing techniques for the preparation of innovative composite structures using thermoplastic materials. The manufacturing of mechanically sustainable composites structures are currently needed. In the recent past, few scientific studies have reported modifying the mechanical properties of thermoplastic material using the metal spraying method by the FFF process. In this study, the acrylonitrile butadiene styrene (ABS-based thermoplastic composites structures have been prepared by Aluminum (Al) metal spray. To investigate the effect of Al spray reinforcement, three input parameters have been selected: the number of sprayed layers (2, 3, and 4), infill pattern (line, triangle, and cubic), and infill density (60, 80, and 100%). The results of the study suggested that maximum strength at peak and maximum strength at break have been observed for composite structures prepared with three number of Al spray layers, triangular-shaped infill printing pattern, and 100% infill density. The genetic algorithm-based multi-objective analysis has been performed for the selection of optimum process parameters. Results of the study were supported with crystallinity analysis using x-ray diffraction (XRD), particle analysis using a scanning electron microscope (SEM), and fracture analysis using optical microscopy.

**Keywords** ABS-Al composites, Al, ABS, FFF, metal reinforcement, tensile strength

## 1. Introduction

Additive manufacturing (AM) or 3D printing technology is used for the fabrication of complex structures by depositing materials layer-by-layer on a build platform (Ref 1). AM processes facilitate the manufacturing of prototypes in less time and quickly fabricate complex structures than conventional manufacturing methods in the commercial sectors (Ref 2). In the last 10 years, the use of AM processes in different sectors (automobile, manufacturing, aerospace, construction, and electronics) has been drastically increased due to better properties comparatively to fabrication processes which are done with the automation process with very less human interventions (Ref 3). The products manufactured using this technique have a significant advantage as it has less weight than a conventional method; thus, it may be successfully implied to the components that require substantially less weight (e.g., aeronautical and

automobile sectors). Also, the structures made using this technology are jointless, which results in the better printing of any complex or intrinsic structure (Ref 4). Due to much flexibility in 3D printing technology, it is easy to change their design very easily using computer-aided design (CAD) software without changing any hardware specifications in a short span of time (Ref 5). The first step involves in 3D printing is to create a CAD model using any CAD software and save it in standard tessellation language (.STL) file format. In the .STL file, the model is converted to triangular facets (Ref 6). The next step is slicing and setting up input parameters like layer height, pattern design, orientation, etc. These input parameters and slicing are performed using slicing software packages. The final step is to print using a 3D printer among various techniques are that available for 3D printing like FFF (Ref 7), stereolithography (SLA) (Ref 8), selective laser sintering (SLS) (Ref 9), and laminated object manufacturing (LOM) (Ref 10), etc. With increasing experimentation, research, and applications of 3D printing in other sectors, the material requires some enhanced properties to match the requirements. Previous researchers have reported outstanding ways of processing composite preparation by using particles and fibers for making mechanically sustainable composite structures. In the recent past, graphene oxide (GO) and reduced graphene oxide (rGO) were reinforced with different thermoplastic polymers using other techniques (vacuum infiltration, casting, spray deposition, solution mixing, dip coating, extrusion, and melt mixing) to check the effect on the mechanical properties of final fabricated product (Ref 11). According to previous research, primary recycling has been done with polyamide 6 (PA6) to enhance mechanical strength using extrusion and 3D printing technology (Ref 12). Many studies have suggested that reinforcement

**Piyush, Raman Kumar, and Jasgurpreet Singh Chohan**, Department of Mechanical Engineering, Chandigarh University, Mohali, Punjab 140413, India; **Ranvijay Kumar** and **Nishant Ranjan**, Department of Mechanical Engineering, Chandigarh University, Mohali, Punjab 140413, India; and University Centre for Research and Development, Chandigarh University, Mohali, Punjab 140413, India. Contact e-mail: ranjan\_nishant92@hotmail.com.

of thermoplastic with different materials increases mechanical properties compared to the virgin polymer matrix. Reinforcement of thermoplastic polymers using twin-screw extruders with other fillers helps to improve their mechanical properties for final product fabrication using 3D printing technology. The previous studies have been reported that reinforcement of Al in thermoplastic has been significantly tuned the mechanical properties of the ABS and PA6 thermoplastics (Ref 13). The fracture morphology of the 3D printed part is one of the most important concerns which decided the mechanical properties (Ref 14). The 3D printing was processed with the combination of polylactic acid (PLA), wood fiber (WF), and Poly (methyl methacrylate) (PMMA). At the optimum reinforcement ratio, a notable increase in tensile and bending strength was reported (Ref 15). The addition of Bromine (Br) in PLA has been significantly enhanced the stiffness by 27% (Ref 16). In addition, the reinforcement of ZnO particles increased the crystallinity of nanocomposite (Ref 17). The addition of the WF has been significantly tuned the mechanical properties of prepared composite structures (Ref 18). In the previous research work, multiple layers of Al were sprayed on the PLA matrix. Reinforced PLA-Al specimens have resulted in better mechanical properties than the specimen prepared using virgin PLA (Ref 19). Previous studies have reported the reinforcement of glass fibers (GF) in polypropylene (PP) feedstock filament which was fabricated using the screw extrusion technique. The results of the study have been suggested that the reinforced filaments provided better mechanical properties as compared to virgin material (Ref 20).

It is evident from the literature that previous investigators have used different tools and techniques to maintain the mechanical properties of the composites structures prepared by 3D printing processes. Previously, less has been reported for the metal spray addition between thermoplastic layers by AM to maintain better properties. As with the higher demand of 3D printing in every industry for various applications having different expectations from end products in terms of strength, appearance, etc., materials and techniques must be compatible. In this study, an attempt has been made to improve the mechanical properties of ABS-printed using FFF with the reinforcement of sprayed Al metal.

## 2. Materials and Method

ABS filament having a diameter of 1.75 mm was used as printing material (Purchased from 3Idea Technology, China). For reinforcement of Al on the ABS matrix, 99.5% pure Al aerosol spray (Make: Wurth India Ltd, India) was used (having a usage limit of temperature up to 300°C). For conducting the experiments, samples were prepared according to ASTM D 638 type IV standards. The dimensional specification of the ASTM D 638 type IV standard is shown in Fig. 1. Reinforcement of Al spray between the ABS layers was performed using the spraying method. For reinforcement of Al on custom layers, the Al spray was performed manually. An acrylic type of mist spray has been used for this research work. To maintain the uniformity of Al in every spray, pilot tests were performed, and it has been observed that on every single push of the spray can, it is spraying approximately 65 mg of Al. The exact quantity of Al spray is performed on every reinforced layer.

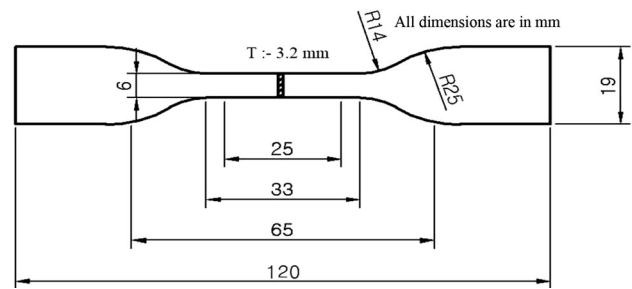


Fig. 1 ASTM D638 Type IV dimensional specifications

## 3. Experimentation

### 3.1 Preparation of ABS-Al Composite Structures

Based on the FFF technique, 3D printing of samples was performed using PRUSA i3 MK2 3D printer (maximum build plate temperature 110°C, extruder temperature 270°C, nozzle diameter 0.4 mm). Reinforcement of Al was performed using the spray method. In performing the process, 3D printing was paused for spraying and resumed again after completing the spraying process. The experimentation process is shown in Fig. 2. To fabricate a composite structure as per ASTM D638 type IV, specimens CAD software named Solidworks 2016 software package was used. Slicing of the 3D model and input parameters were set using Ultimaker Cura 4.5 software package. In the printing of samples, some constants and variables were used as input parameters.

The constant parameters used for printing samples are the layer height of 0.1 mm, printing temperature of 240°C, build plate temperature of 80°C and printing angle of 45°. These constant parameters have been selected based on the previously reported studies (Ref 21, 22). The variable printing parameters used in experimentation were the number of reinforced Al layers, infill density and infill pattern. 2, 3 and 4 number of reinforced Al layers. Three infill patterns, linear, triangular and cubic, were used as three designs print differently with different infill shapes. Infill densities were selected as 60, 80, and 100% to know about the impact of Al reinforcement at different porosity. The design of the experiment (DOE) was prepared using Taguchi L9 (3<sup>3</sup>) orthogonal array for the development of ABS-Al composite structures (Table 1).

The ABS-Al composite structures with each of 2, 3 and 4 sprayed Al layers were prepared by the FFF process. Three samples were prepared to have two layers of Al, in such samples the first layer was sprayed at 33% completion of printing or the 13th layer of the sample and the second layer was sprayed at 66% completion or the 26th layer. The next three samples were prepared using the three spray layers. In such samples, the first layer was sprayed at 25% completion (10th layer), the second at 50% completion (20th layer) and the third layer at 75% completion (30th layer). Similarly, the last three samples were prepared with 4 Al sprayed layers. The first layer was sprayed at 20% completion (8th layer), the second layer at 40% completion (16th layer), the third layer at 60% completion (24th layer) and the fourth and last layer was sprayed at 80% completion of printing or on 32nd layer. The spray interval is shown in Table 2. An SEM image that was taken at a magnification of 1000x is shown in Fig. 3. It was observed that very fine Al particles are equally distributed in

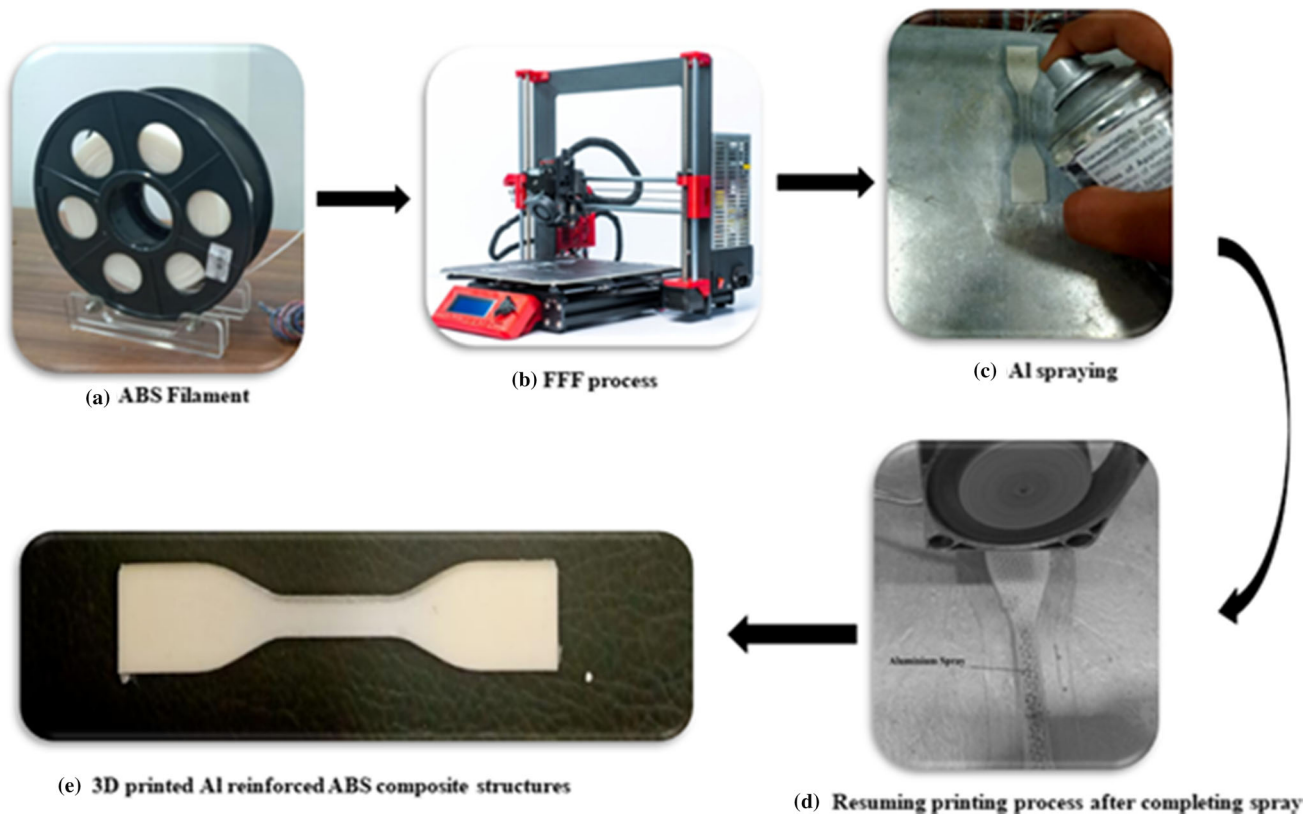


**Fig. 2** (a) ABS Filament, (b) FFF process (c) Al spraying, (d) Resuming printing process after completing spray, (e) 3D printed Al reinforced ABS composite structures

**Table 1** Experimental design for FFF process

Exp No.	No. of Al layers	Infill pattern	Infill density, %
1	2	Line	60
2	2	Triangle	80
3	2	Cubic	100
4	3	Line	80
5	3	Triangle	100
6	3	Cubic	60
7	4	Line	100
8	4	Triangle	60
9	4	Cubic	80

**Table 2** Interval for Al spray process during FFF process

Al spray layer	Samples with 2 layers	Samples with 3 layers	Samples with 4 layers
1st layer	33% (13th layer)	25% (10th layer)	20% (8th layer)
2nd layer	66% (26th layer)	50% (20th layer)	40% (16th layer)
3rd layer	...	75% (30th layer)	60% (24th layer)
4th layer	...	...	80% (32nd) layer

the whole surface and closely attached, contributing to the sample's mechanical strength. Al particles were present in micrometer (2 different particle sizes of Al particles are shown in SEM image) varies from 2 to 8  $\mu\text{m}$  with irregular shape (coin-like structure, cubic and spherical) (see Fig. 3).

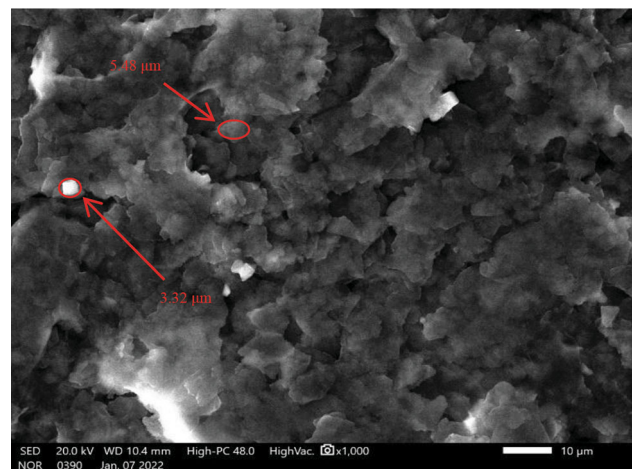
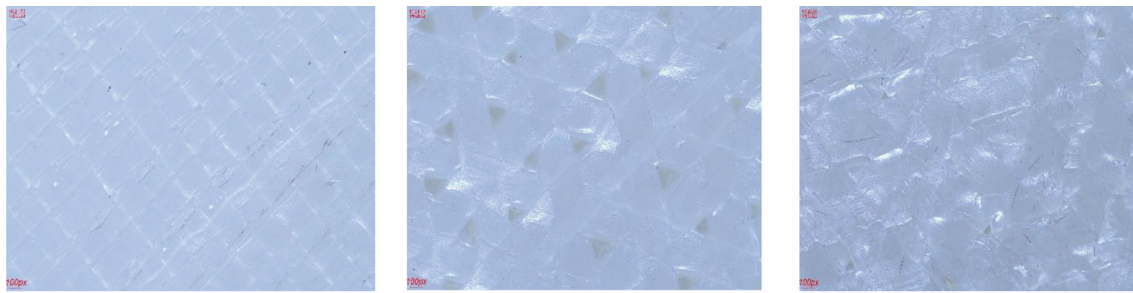


**Fig. 3** SEM image of Al spray at 1000x magnifications

There are a total of nine samples prepared according to parameters shown in Table 1 (repeated 3 times for each sample to reduce the experimental errors). Per Table 1, all nine samples were prepared using a modified FFF process, and the internal structure of infill patterns (Line, triangle and cubic) are shown in Fig. 4.

### 3.2 Tensile Testing

Tensile strength evaluation was performed on the universal tensile machine (UTM) to determine the material's mechanical



(a) Line pattern

(b) Triangle pattern

(c) Cubic pattern

**Fig. 4** Internal structure of prepared parts prepared using line, triangle and cubic infill

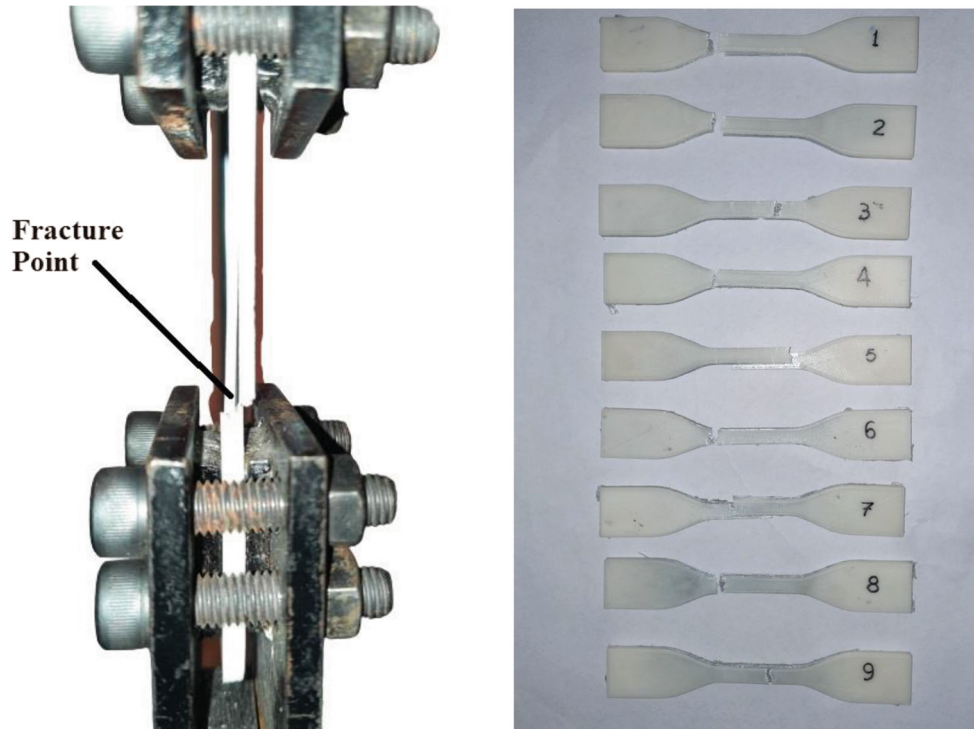


**Fig. 5** (a) Sample undergoing tensile test, (b) Fractured samples

properties. It was used for the quantitative value of force needed to break the specimen made of homogeneous material or any other composite material. The UTM manufactured by Shanta Engineering India, having a maximum capacity of 5000 N, was used. Three samples made upon each experimental condition were tested, and their average value was evaluated.

Figure 5(a) shows samples undergoing a tensile test, and samples fractured after tensile testing are shown in Fig. 5(b). The outcomes achieved from tensile testing are tensile strength at peak, tensile strength at break, percentage elongation at peak and percentage elongation at break. These results obtained from tensile testing are shown in Table 3.

### 3.3 Photomicrographic and XRD Analysis

The optical photomicrographic analysis is an experimental process that analyses different magnified images using an

optical microscope. For this research work analysis, 100x magnified images were captured using an optical microscope (Model No: SMZ745T; Manufacturer: Nikon) and roughness and 3D rendering using “Gwyddion software version 2.59”. After that, with the help of the XRD machine (Model: D8 Advance eco; Manufacturer; Bruker Scientific Instruments, Billerica, Massachusetts) best and worst sample according to tensile strength has been analyzed.

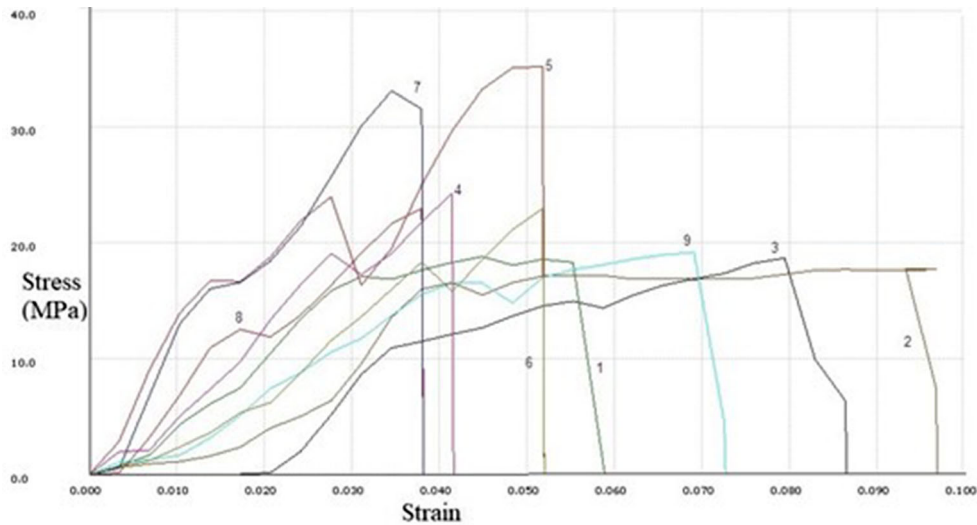
## 4. Results and Discussion

### 4.1 Tensile Properties

Table 3 shows the tensile properties of ABS-Al hybrid composite structures prepared by the modified FFF process.

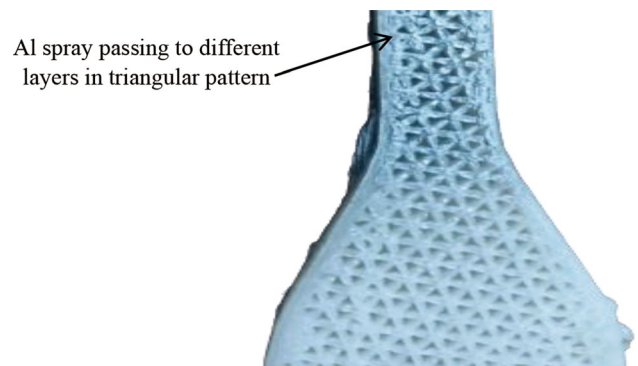
**Table 3 Tensile properties of ABS-AI composites structures**

Sample no.	Strength at peak, MPa	Strength at break, MPa	% Elongation at peak	% Elongation at break
1	18.74	16.87	8	9
2	17.80	16.02	10	10
3	18.87	16.98	4	6
4	24.82	22.34	4	4
5	35.29	31.76	5	5
6	23.06	20.75	3	4
7	34.63	31.17	3	4
8	23.47	21.12	5	5
9	19.23	17.31	7	7

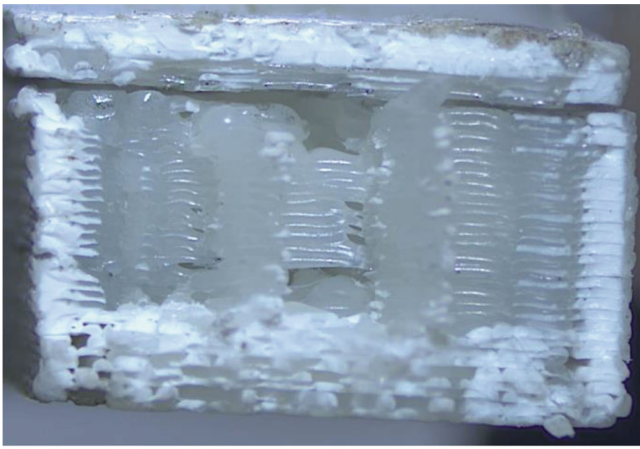
**Fig. 6** Stress and strain plots for fractures ABS-AI composite structures

The maximum tensile strength was observed for sample 5, whereas the minimum was for sample 2. Based upon the results given in Table 3, the stress versus strain curves have been plotted. The observed value of tensile properties is given in Table 3, and the stress vs strain graph is shown in Fig. 6. The maximum strength at peak and maximum strength at break were observed for sample no. 5, having input parameters as three reinforced Al sprayed layers, triangular-shaped infill printing pattern and 100% infill density, i.e., maximum infill density. Based on Table 3, sample 5 exhibited better mechanical strength because of the triangular shape with 100% density enhanced maximum strength compared to others due to better bonding between layers. Al gets deposited between porous regions formed due to triangular patterns and increases its tensile properties. The triangular infill pattern facilitating this porous environment for the passing of Al in corresponding layers is shown in Fig. 7.

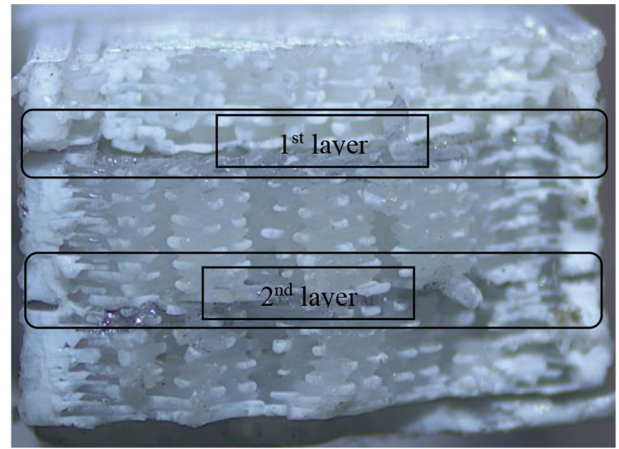
The minimum values of tensile strength at break and tensile strength at the peak were observed for sample no. 2, having input parameters as two sprayed Al layers, triangular infill pattern and 80% infill density. The triangular infill provides more porosity and hence more hollow space, minimum no. of reinforced Al layers resulted in low tensile strength values. All the samples prepared with a minimum number of reinforced Al layers (i.e., two layers) have shown lesser tensile strength due to only two Al layers.

**Fig. 7** Scope of passing to different layers in a triangular pattern

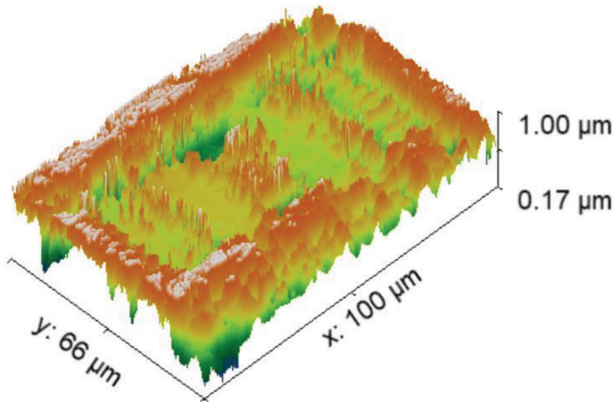
The Al reinforcement in the ABS layers has increased its strength and reduced its elongation capacity. The maximum elongation at peak and break were observed for sample no. 2, as a smaller number of reinforced Al layers resulted in low strength and perhaps increased its ductility. Minimum elongation at peak and break is observed at sample 7, with 4 Al layers and 100% infill density.



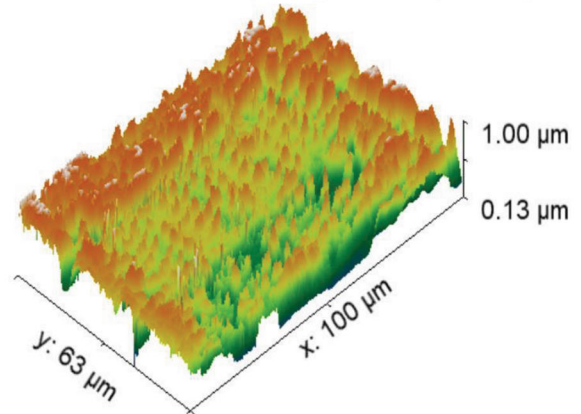
(a) x100 magnification image of fractured part of worst tensile (Sample no. 2) strength



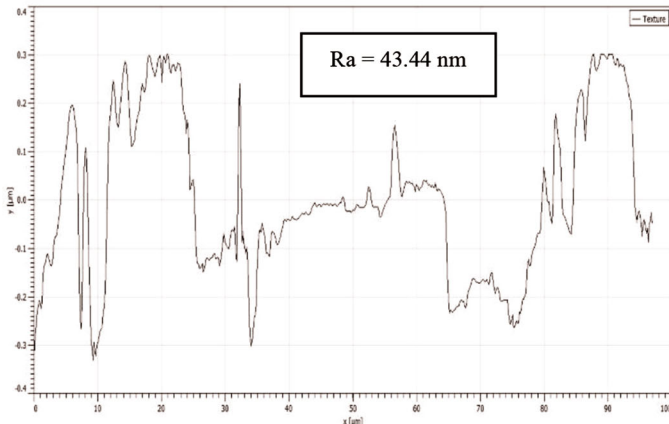
(b) x100 magnification image of fractured part of best tensile (Sample no. 5) strength



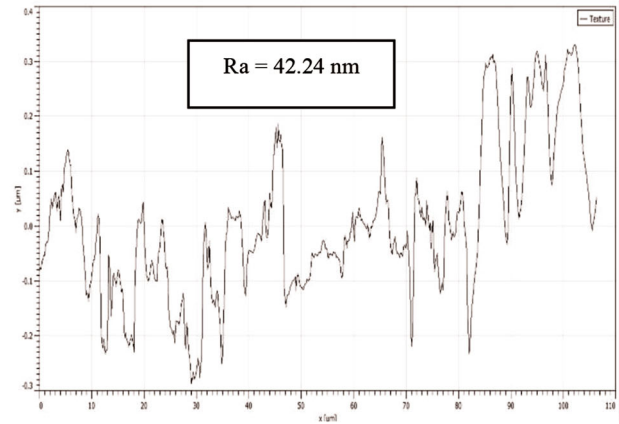
(c) 3D rendering image of the surface of the worst tensile (Sample no. 2) strength



(d) 3D rendering image of the surface of the best tensile (Sample no. 5) strength



(e) Graphical view of surface roughness of fractured part of worst tensile sample



(f) Graphical view of surface roughness of fractured part of best tensile sample

**Fig. 8** 100x Optical image, 3D rendering image and surface roughness graph sample no. 2 and sample no. 5

#### 4.2 Photo-Microstructure Properties

The samples manufactured on experimental condition 5 had the best tensile results based on tensile strength results, whereas

experimental run no. 2 had the minor tensile strength of value. For the fracture analysis, the fractured portion of the worst and best tensile strength samples were captured at 100x magnification, as shown in Fig. 8(a) and (b). According to Fig. 8(a) and

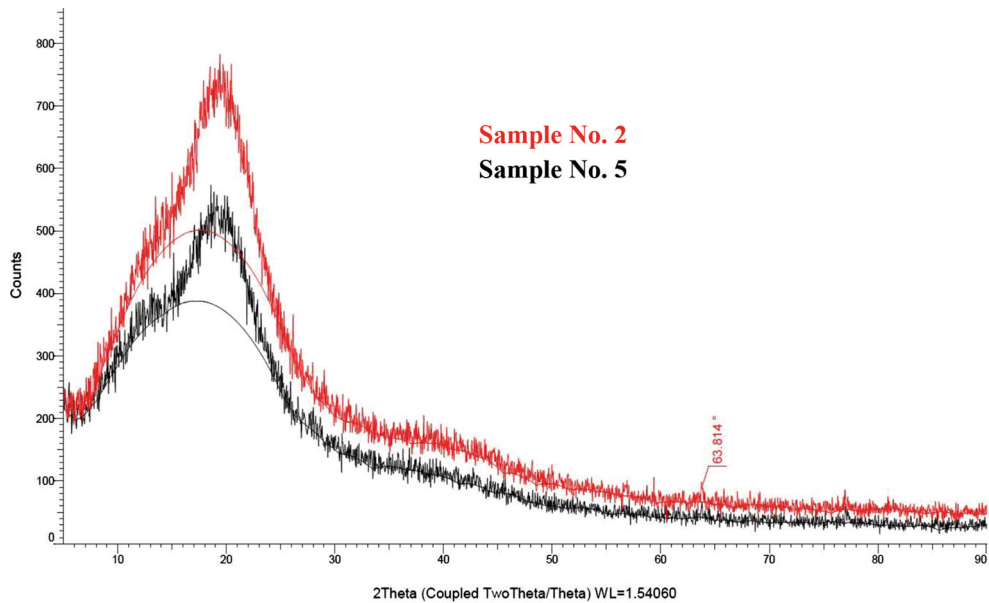


Fig. 9 XRD curves for sample no. 2 and sample no. 5

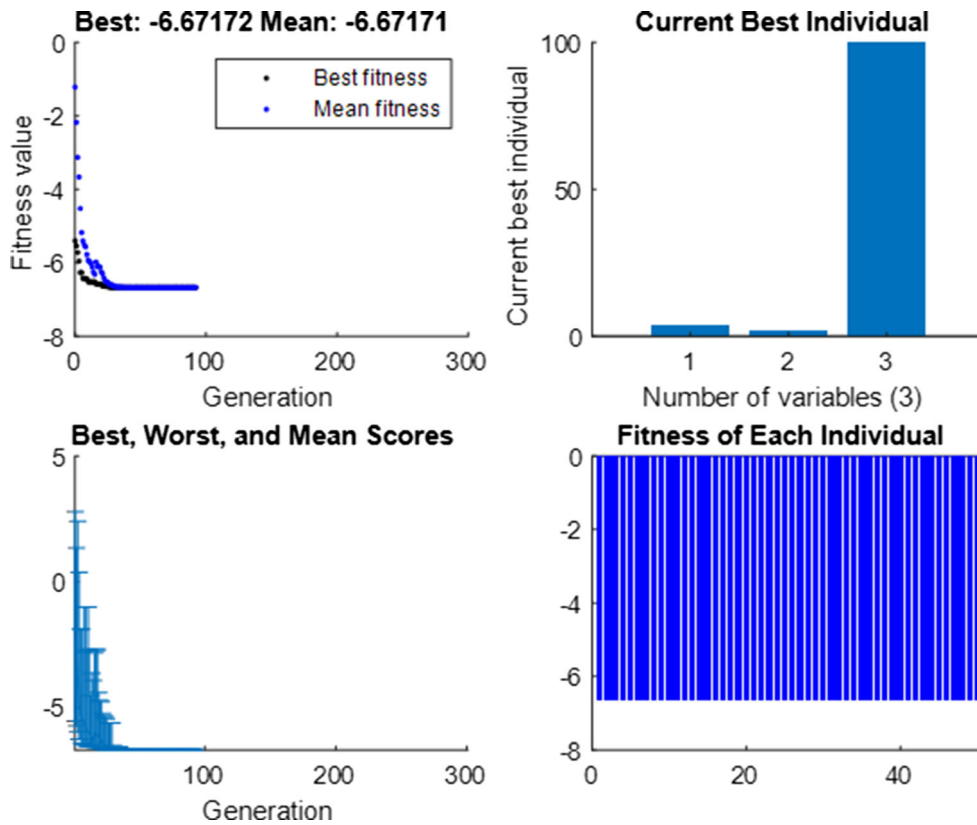


Fig. 10 Genetic algorithm output plots

(b) observed, Al-coating distribution in the tensile sample are equally distributed in sample 5, but in the case of sample no. 2, the no. of Al-coating is not adequately distributed. It is one of the most important reasons that support that tensile strength results because equally distribution of no. of layers concerning Al-coating provides/gives more strength than other samples. 3D rendering images are shown in Fig. 8(c) and (d) for the fractured parts corresponding to experimental run no. 2

(minimum tensile strength) and 5 (maximum tensile strength) that were prepared by using optical photo microstructure that is shown in Fig. 8(a) and (b) with the help of “Gwyddion software version 2.59”. Based on Fig. 8(c) and (d), a 3D image of the fractured surface is similar over the entire area of experimental run no. 5, whereas in the case of sample no. 2 has unequal surface distributions. Lastly, by using “Gwyddion software version 2.59”, average surface roughness has been

determined, and the graph of the surface roughness is shown in Fig. 8(e) and (f). The average surface roughness ( $R_a$ ) value in sample no. 2 was 43.44 nm, whereas 42.44 nm in the experimental run no. 5. Lower  $R_a$  shows better mechanical blending, providing better mechanical (tensile) strength.

**Table 4 Function values and outputs of individual maximization and multi-objective**

	X (1)	X (2)	X (3)	Function value
PS <sub>MAX</sub>	3.590429	1.74323	100	37.38123
BS <sub>MAX</sub>	3.591457	1.743774	100	33.64427
PE <sub>MAX</sub>	2	1.785906	73.99827	10.26625
BE <sub>MAX</sub>	2.000033	1.833359	70.00481	10.29143
Multi-objective	3.963539	1.952382	100	6.67172

Based on tensile strength results in the best and worst sample has been analyzed by XRD from 5° to 90° with 2135 steps. According to Fig. 9, it has been observed that sample 2 and sample 5 has approximately similar patterns; this may be due to the higher amount of ABS polymers contained are present on the top of the sample surface. According to the XRD library file, Fig. 10 graph is closer to ABS thermoplastic polymers. In both cases, it was observed that only one peak in sample no. 2 (63.814°) that may be present possibly due to some foreign particles are present in that sample. ABS is normally an amorphous material and according to XRD analysis sample, no. 2 and sample no. 5 are 74.5% and 74.4% amorphous, respectively. So XRD analysis confirms that working materials are ABS thermoplastic polymers.

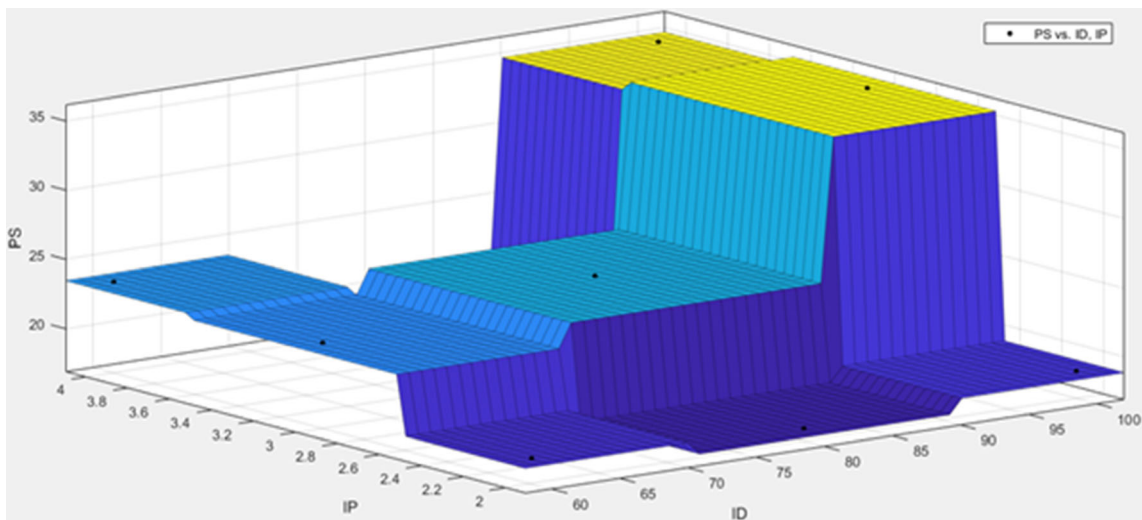


**Fig. 11** Effect of infill density and infill pattern on peak strength

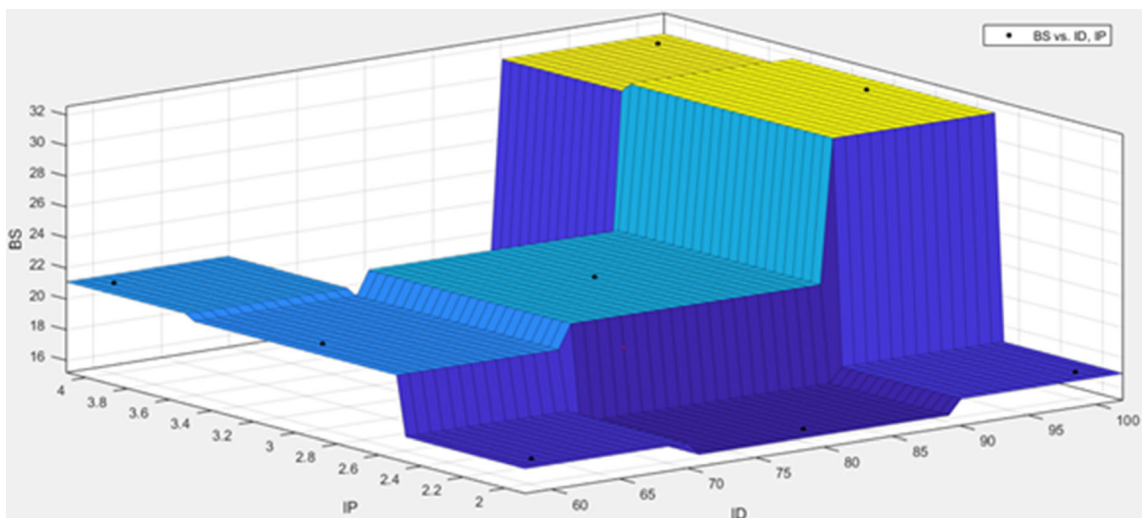


**Fig. 12** Effect of infill density and infill pattern on breaking strength



## 5. Multi-Objective Optimization Using Genetic Algorithm

It has been observed from Table 3 that the tensile properties of all nine samples (prepared under different experimental conditions) are different from each other. Sample no. 5 showed maximum values of 35.29 and 31.76 MPa during measurement of strength at peak and break, respectively. On the other hand, maximum elongation at peak and break was 10% in the case of sample no. 2. Hence, input parameters have a significant impact on tensile strength. During practical applications, all the tensile properties are desirable and hence, there is a need to explore manufacturing conditions where all the tensile properties are maximized. To attain the optimum parametric settings, multi-response optimization must be performed. The present study used experimental data to derive regression equations through Minitab analytical tool. Conclusively, four regression Eqs 1, 2, 3 and 4 were formulated for peak strength, breaking strength, peak elongation, and breaking elongation, respectively.

$$\begin{aligned} \text{Peak Strength} = & 43.54 + 27.63 * X(1) + 15.51 * X(2) \\ & - 2.114 * X(3) - 5.600 * X(1) * X(1) \\ & - 3.683 * X(2) * X(2) + 0.01172 * X(3) * X(3) \\ & - 0.7433 * X(1) * X(2) + 0.1388 * X(1) * X(3) \end{aligned} \quad (\text{Eq 1})$$

$$\begin{aligned} \text{Peak Elongation} = & 13.00 - 20.83 * X(1) + 5.667 * X(2) \\ & + 0.5167 * X(3) + 2.167 * X(1) * X(1) \\ & - 2.333 * X(2) * X(2) - 0.004167 * X(3) * X(3) \\ & + 1.333 * X(1) * X(2) + 0.05000 * X(1) * X(3) \end{aligned} \quad (\text{Eq 3})$$

$$\begin{aligned} \text{Breaking elongation} = & -28.00 - 22.50 * X(1) \\ & + 3.500 * X(2) + 0.2500 * X(3) \\ & + 2.500 * X(1) * X(1) - 1.500 * X(2) * X(2) \\ & - 0.002500 * X(3) * X(3) \\ & + 1.000 * X(1) * X(2) + 0.05000 * X(1) * X(3) \end{aligned} \quad (\text{Eq 4})$$

where X (1) is No. of layers X (2) is Infill pattern X (3) is Infill density

These equations can be used for the prediction of each tensile property based upon input process parameters X(1), X(2) and X(3). Although, the maximized value for each tensile property can be attained by careful selection of process parameters. However, it is impossible to attain a maximized value of all the tensile properties at single parametric settings as regression equations differ for each tensile property. To solve this multi-response optimization problem, the weights are assigned to each tensile property and combined Eq 5 has been formulated.

### Multi – objective optimization

$$\begin{aligned} = & W_1 * [43.54 + 27.63 * X(1) + 15.51 * X(2) \\ & - 2.114 * X(3) - 5.600 * X(1) * X(1) - 3.683 * X(2) * X(2) \\ & + 0.01172 * X(3) * X(3) - 0.7433 * X(1) * X(2) + 0.1388 * X(1) \\ & * X(3)] - W_2 * [39.21 + 24.85 * X(1) + 13.95 * X(2) - 1.903 * X(3) \\ & - 5.038 * X(1) * X(1) - 3.313 * X(2) * X(2) \\ & + 0.01055 * X(3) * X(3) - 0.6667 * X(1) * X(2) \\ & + 0.1250 * X(1) * X(3)] - W_3 * [13.00 - 20.83 * X(1) \\ & + 5.667 * X(2) + 0.5167 * X(3) + 2.167 * X(1) * X(1) \\ & - 2.333 * X(2) * X(2) - 0.004167 * X(3) * X(3) + 1.333 * X(1) * X(2) \\ & + 0.05000 * X(1) * X(3)] - W_4 * [-28.00 - 22.50 * X(1) + 3.500 * X(2) \\ & + 0.2500 * X(3) + 2.500 * X(1) * X(1) - 1.500 * X(2) * X(2) \\ & - 0.002500 * X(3) * X(3) + 1.000 * X(1) * X(2) + 0.05000 * X(1) * X(3)] \end{aligned} \quad (\text{Eq 5})$$

$$\begin{aligned} \text{Breaking Strength} = & 39.21 + 24.85 * X(1) + 13.95 * X(2) \\ & - 1.903 * X(3) - 5.038 * X(1) * X(1) \\ & - 3.313 * X(2) * X(2) + 0.01055 * X(3) * X(3) \\ & - 0.6667 * X(1) * X(2) + 0.1250 * X(1) * X(3) \end{aligned} \quad (\text{Eq 2})$$

where W<sub>1</sub>, W<sub>2</sub>, W<sub>3</sub>, and W<sub>4</sub> are weights assigned to peak strength, breaking strength, peak elongation, and elongation, respectively. In present experimentation, equal weights were assigned as all the tensile properties are critical for rapid prototyping and functional prototyping applications. After assigning equal weights (W<sub>1</sub> = W<sub>2</sub> = W<sub>3</sub> = W<sub>4</sub> = 0.25), the function values and individual parameter levels are calculated for each response (see Table 4).

This tabular data can achieve maximized output for each response, i.e., peak strength, breaking strength, peak elongation, and elongation. The levels of each input parameter, i.e.,

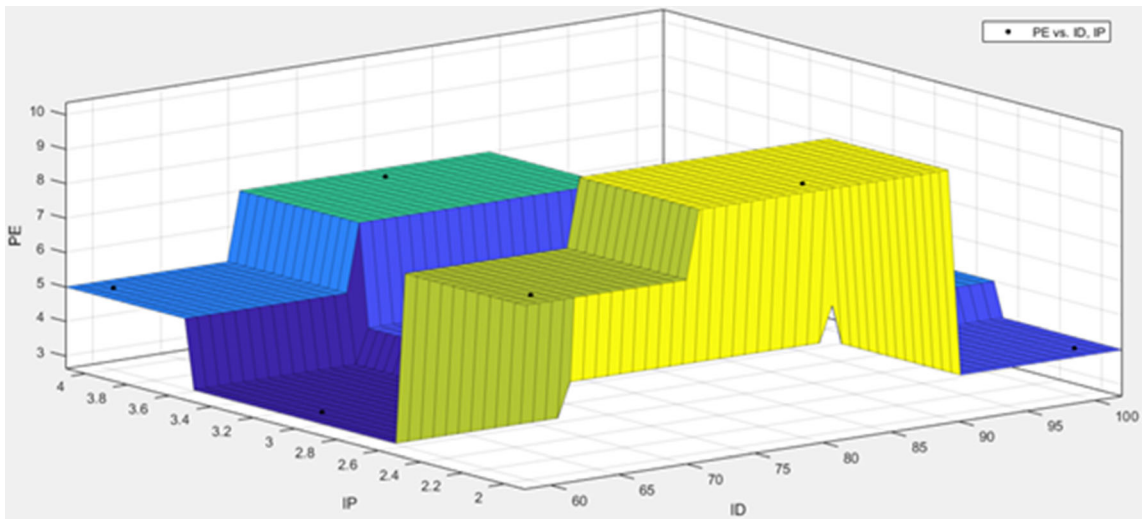


**Fig. 13** Effect of infill density and infill pattern on peak elongation

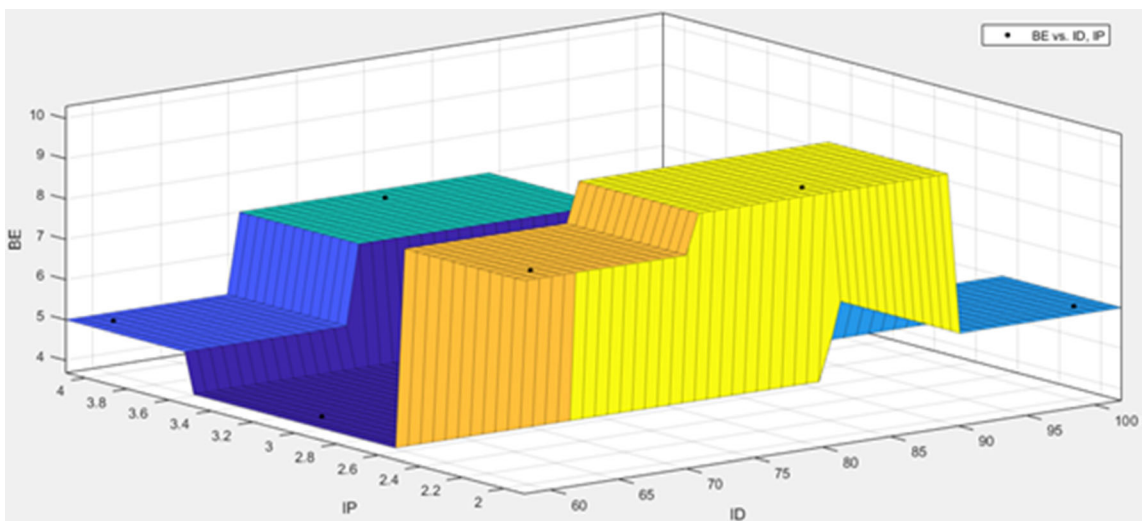


**Fig. 14** Effect of infill density and infill pattern on breaking elongation

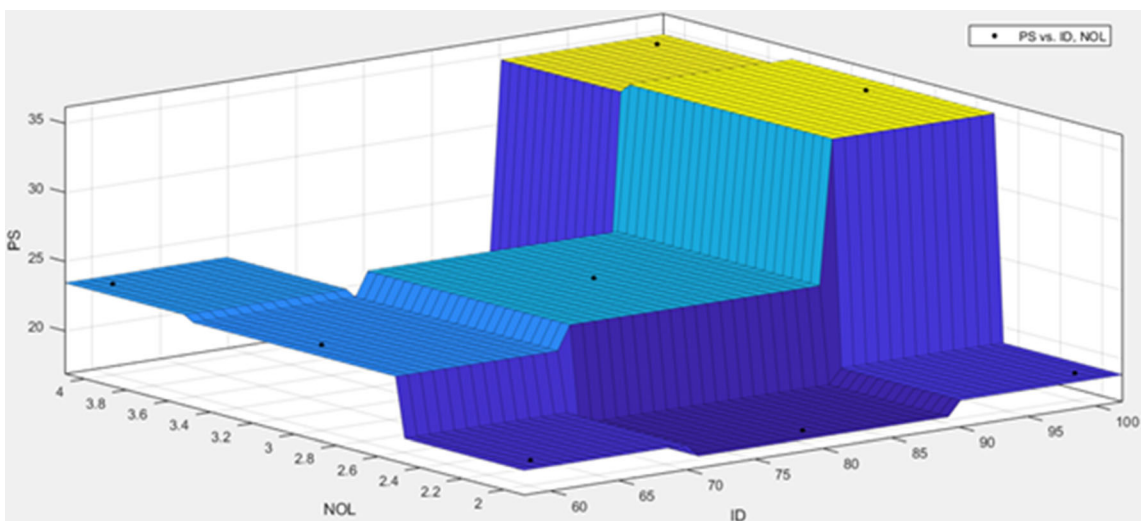


**Fig. 15** Effect of infill density and number of layers on peak strength

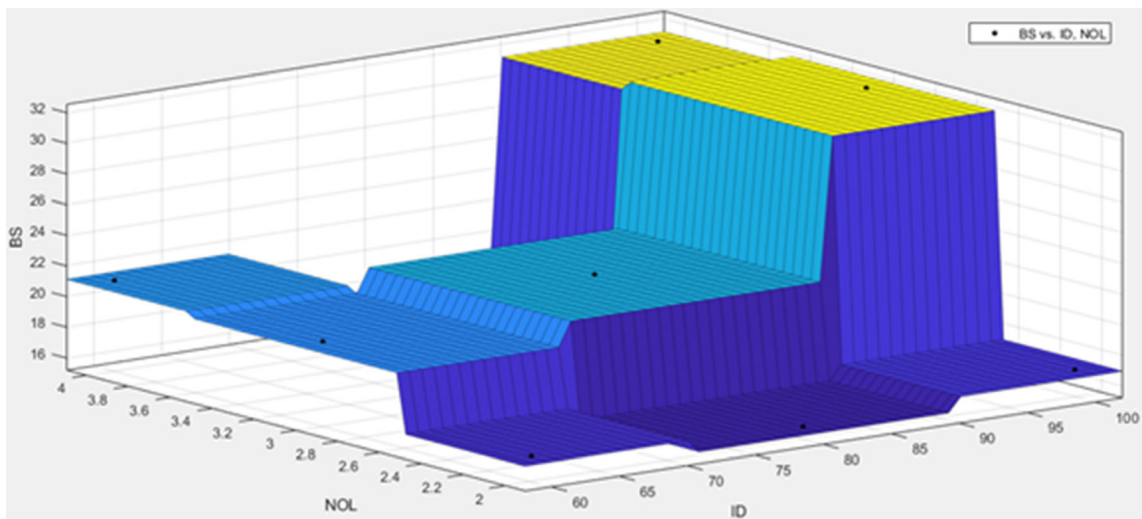


**Fig. 16** Effect of infill density and number of layers on breaking strength

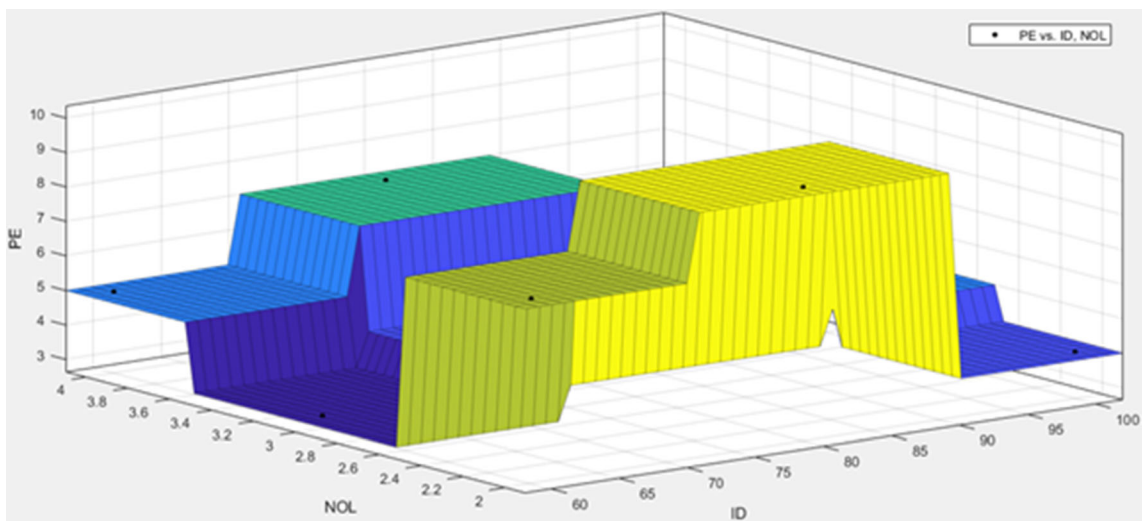


**Fig. 17** Effect of infill density and number of layers on peak elongation

X(1), X(2) and X(3) can be selected to customize the tensile strength. However, in the last row, the multi-objective function value was calculated which along with levels of each input parameter.

These manufacturing conditions would yield a combined maximized value for all the response parameters. Thus, after rounding-off, the optimum parameter settings were 4 layers with triangle pattern and 100% infill density. Genetic algorithm plots in Fig. 10 indicated that the best fitness value of 6.67172 was attained after 100 generations. Furthermore, it can be visualized from Genetic algorithm plots that the best score occurred after 100 generations, whereas mean values were obtained after 35 generations. On the other hand, the worst scores were attained after one generation.

MATLAB has been used to investigate the impact of manufacturing conditions on response. Figure 11 plots the effect of infill density and infill pattern on peak strength. In contrast, Fig. 12 shows the impact of infill density and infill pattern on the breaking strength of 3D printed polymer composite parts. It can be deduced that a triangle pattern with

100% density yields maximum peak and breaking strength. The ABS polymer parts reinforced with Al spray can be strengthened by using these manufacturing conditions. Generally, the increase in density positively impacts tensile strength, which has also been experienced during the present examination.

Figure 13 and 14 plots the effect of variable infill density and infill pattern on peak and breaking elongations, respectively. It was noticed that maximum values of breaking peak and elongation occur at 75-95% infill density with a triangle pattern. The minimum values of breaking elongation occur at 100% density with a cubic pattern. The combined effect of 100% density and cubic pattern reduces the flexibility of the polymer.

Figure 15 and 16 shows the variation in peak strength and breaking strength with several Al layers and infill density. Similar trends have been observed in both plots, i.e., density in the range of 90-100% with three layers yield maximum response. Previous studies have also observed that the addition of metal particles inside 3D printed polymer layers strengthened the parts. Moreover, the additional support is provided by

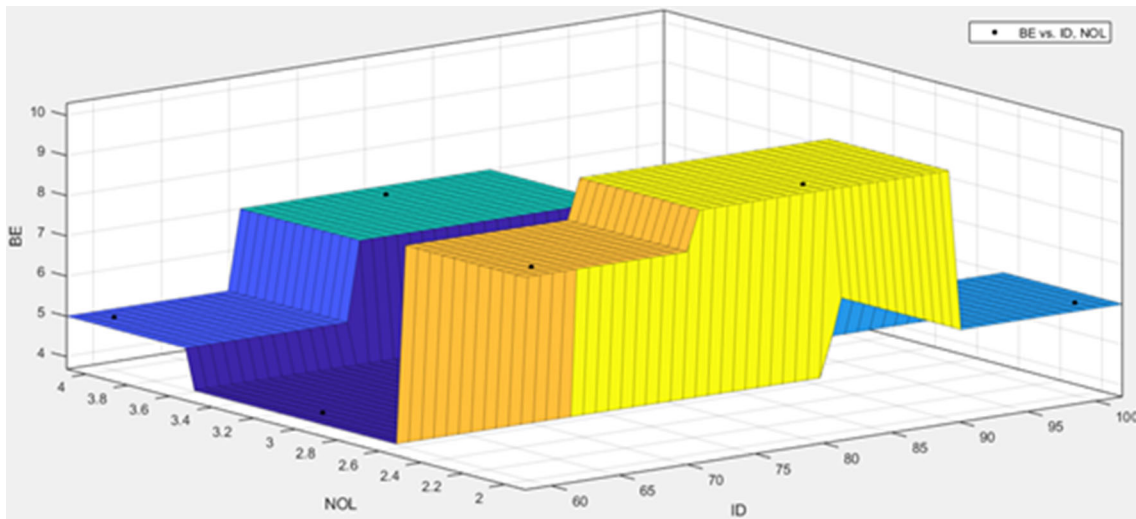


**Fig. 18** Effect of infill density and number of layers on breaking elongation

higher density. In the present study, the metal spray is accommodated by minor voids in layers which provided required bonding strength to resist the tensile loading.

Figure 17 and 18 show the variations of peak elongation and break elongation with changing infill density and number of layers, respectively. It has been noticed that there is an almost similar impact on both the response parameters. A smaller number of layers with the range of 75-90% infill density exhibit maximum peak and breaking elongation.

The individual responses of each parameter have been plotted and discussed. In general, the higher values of infill density and triangle pattern yield higher tensile strength values. The number of layers must be smaller to attain maximized elongation values, whereas layers can be increased to improve the peak and breaking strength. Genetic algorithms have predicted similar findings. The findings of this study can be used to design and manufacture functional prototypes with customized tensile strength. The selection of metal spray concentration and layer count can also be varied to attain desired output.

## 6. Conclusions

Followings are the conclusions of this study:

- The Al spray reinforcement in between the ABS layers has been increased tensile strength. Maximum strength at peak and maximum strength at break are obtained in sample no. 5, having input parameters 3 Al spray layers, triangular-shaped infill printing pattern and 100% infill density.
- The minimum values of tensile strength at break and tensile strength at the peak has been observed for sample no. 2, having input parameters as 3 Al layers, triangular infill pattern and 80% infill density. This sample has a minimum value due to less density and less Al-sprayed layer than other combinations.
- Per the discussion of response optimization, the higher values of infill density and triangle pattern yield higher tensile strength values. To attain maximized elongation

values, the number of layers must be smaller, whereas layers can be increased to improve the peak and breaking strength. Genetic algorithms have predicted similar findings.

## Acknowledgment

Authors are highly thankful to the Center for Manufacturing Research, Guru Nanak Dev Engineering College, Ludhiana and University Center for Research and Development, Chandigarh University for technical/experimental assistance in this research work.

## References

1. M.D. Meisner, and W.N.M. Robin, Three-Dimensional Modelling and/or Manufacturing Apparatus, and Related Processes. U.S. Patent Application No. 10/137,636
2. P. Wu, J. Wang, and X. Wang, A Critical Review of the Use of 3-D Printing in the Construction Industry, *Autom. Constr.*, 2016, **68**, p 21–31
3. M.S. Khan and S.B. Mishra, Minimizing Surface Roughness of ABS-FDM Build Parts: An Experimental Approach, *Mater. Today Proc.*, 2020, **26**, p 1557–1566
4. Y. Gao et al., Modeling of Material Removal in Magnetic Abrasive Finishing Process with Spherical Magnetic Abrasive Powder, *Int. J. Mech. Sci.*, 2020, **177**, p 105601
5. C.K. Chua and K.F. Leong, *3D Printing and Additive Manufacturing: Principles and Applications (with Companion Media Pack)-of Rapid Prototyping*, World Scientific Publishing Company, Singapore, 2014
6. Roscoe, L. Stereolithography Interface Specification. America-3D Systems Inc 27.2020 (1988): 10
7. A.G. Rebenaque and I. González-Requena, Study of Bending Test of Specimens Obtained Through FDM Processes of Additive Manufacturing, *Procedia Manuf.*, 2019, **41**, p 859–866
8. B.T. Phillips et al., Additive Manufacturing Aboard a Moving Vessel at Sea Using Passively Stabilized Stereolithography (SLA) 3D Printing, *Addit. Manuf.*, 2020, **31**, p 100969
9. P. Obst et al., Failure Criterion for PA12 SLS Additive Manufactured Parts, *Addit. Manuf.*, 2018, **21**, p 619–627
10. M. Krinitcyn et al., Laminated Object Manufacturing of in-situ Synthesized MAX-Phase Composites, *Ceram. Int.*, 2017, **43**(12), p 9241–9245

11. D.N. Trivedi and V.R. Nikunj, Graphene and its Application in Thermoplastic Polymers as Nano-Filler-A Review, *Polymer*, 2021, **240**, p 124486
12. R. Singh, R. Kumar, N. Ranjan, R. Penna, and F. Fraternali, On the Recyclability of Polyamide for Sustainable Composite Structures in Civil Engineering, *Compos. Struct.*, 2018, **184**, p 704–713
13. R. Singh, R. Kumar, and I.P.S. Ahuja, Friction Welding for Functional Prototypes of PA6 and ABS with Al Powder Reinforcement, *Proc. Natl. Acad. Sci. India Sect. A*, 2020, **91**(2), p 351–359.
14. K.R. Hart and D.W. Eric, Fracture Behavior of Additively Manufactured Acrylonitrile Butadiene Styrene (ABS) Materials, *Eng. Fract. Mech.*, 2017, **177**, p 1–13.
15. L. Wan and Z. Yanhua, Jointly Modified Mechanical Properties and Accelerated Hydrolytic Degradation of PLA by Interface Reinforcement of PLA-WF, *J. Mech. Behav. Biomed. Mater.*, 2018, **88**, p 223–230.
16. F. Alam et al., Microarchitected 3D Printed Polylactic Acid (PLA) Nanocomposite Scaffolds for Biomedical Applications, *J. Mech. Behav. Biomed. Mater.*, 2020, **103**, p 1035.
17. R.C. Nonato et al., Nanocomposites of PLA Containing ZnO Nanofibers Made by Solvent Cast 3D Printing: Production and Characterization, *Eur. Polymer J.*, 2019, **114**, p 271–278.
18. M. Kariz et al., Effect of Wood Content in FDM Filament on Properties of 3D Printed Parts, *Mater. Today Commun.*, 2018, **14**, p 135–140.
19. R. Kumar et al., Metal Spray Layered Hybrid Additive Manufacturing of PLA Composite Structures: Mechanical, Thermal and Morphological Properties, *J. Thermoplast. Compos. Mater.*, 2020 <https://doi.org/10.1177/0892705720932622>
20. G. Sodeifian, G. Saghar, and A.Y. Ali, Preparation of Polypropylene/Short Glass Fiber Composite as Fused Deposition Modeling (FDM) Filament, *Res. Phys.*, 2019, **12**, p 205–222.
21. S. Khabia and K.J. Kamlesh, Influence of Change in Layer Thickness on Mechanical Properties of Components 3D Printed on Zortrax M 200 FDM Printer with Z-ABS Filament Material & Accucraft i250+ FDM Printer with Low Cost ABS Filament Material, *Mater. Today Proc.*, 2020, **26**, p 1315–1322.
22. F. Saenz et al., Influence of 3D Printing Settings on Mechanical Properties of ABS at Room Temperature and 77 K, *Addit. Manuf.*, 2021, **39**, p 101841.

**Publisher's Note** Springer Nature remains neutral with regard to jurisdictional claims in published maps and institutional affiliations.